A numerical approach to study the impact of packing density on fluid flow distribution in hollow fiber module

Jan Günther[a,b], Philippe Schmitz[a,*], Claire Albasi[b], Christine Lafforgue[a]

[a] Laboratoire d'ingénierie des Systèmes Biologiques et des Procédés, UMR INSA CNRS 5504, UMR INSA INRA 792, 135 avenue de Rangueil, 31077 Toulouse cedex 04, France
[b] Laboratoire de Génie Chimique, UMR CNRS 5503, 5 rue Paulin Talabot, BP 1301, 31106 Toulouse cedex 01, France

Keywords:
Filtration
Computational Fluid Dynamics
Hollow fiber
Packing density

A B S T R A C T

The aim of this study was to analyze the influence of hollow fiber module design, specially packing density, and filtration operating mode on the filtration performance. In order to perform this analysis, a model based on the finite element method was used to simulate numerically the flow and filtration velocity along the fiber. An annular region of fluid surrounding the fiber was considered in order to account for the packing density Φ of the module. The originality of this approach lies in the study of fiber density effect on the hydrodynamic conditions, both for inside/out (IO) and outside/in (OI) filtration modes. The numerical simulations of fluid flow have shown a modification of the axial filtration velocity profile with packing density. When the density of fibers was high, filtration took place preferentially in the bottom of the fiber. In contrast, when the packing density was low, permeate flow was higher at the top of the fiber, i.e. the filtration module. Two experimental hollow fiber modules with two packing densities were tested and showed good agreement with the numerical data. These results underline the variations of filtration velocity along the fiber that will allow some predictions on fouling deposit to be done.

1. Introduction

Hollow fiber membranes have become ubiquitous in many fields such as waste water treatment [1–3], biomedical engineering [4] and processing of beverages [5] because of their low manufacturing costs and simple handling. Moreover, one of the main advantages of this filtration configuration is the high membrane area per volume unit of module in comparison with other configurations of membranes. However, the major consequence of maximizing the membrane surface area per unit volume is an increase of the packing density of the hollow fibers. In submerged hollow fiber membrane processes, modules need voids among the fibers. These spaces not only become the path of up-flow but also facilitate mass transfer through fibers. Another consequence of high packing density could be increased fouling due to the unfavorable hydrodynamic conditions within the fiber bundles [6]. The filtration performance of a hollow fiber bundle depends on operating parameters such as the operating flux in constant flux mode or operating pressure in constant pressure mode as well as the packing density. Since high fiber density results in a poorer inter-fiber hydrodynamic environment [7,8], optimization of fiber density may be relevant to improve the filtration performance of a submerged system.

Few authors have tried to evaluate the performance of individual fibers experimentally in a submerged hollow fiber bundle [9,10]. The fibers located at different positions in the bundle behave differently as they are exposed to different hydrodynamic conditions. Yeo and Fane [10] described an experimental model bundle of nine fibers, which allowed the filtration flux of individual fibers to be measured. They found that the inner fibers (centre) performed very poorly compared to the external ones (corner and sides). A number of two-dimensional models [6,11–14] of varying degrees of complexity or simplification can be found in the literature. They model the flow in membranes or thin channels with permeable walls. Karode [11] presented an analytical solution for the pressure drop in fluid flow in a rectangular slit and cylindrical tube with a porous wall at constant wall velocity. He found analytical expressions for pressure drop as a function of wall permeability, channel dimension, axial position and fluid properties. Nassehi [14] considered various methods to link the Navier Stokes and Darcy equations in a solution scheme, in order to simulate the flow field in crossflow membrane filtration in a porous tube. The interest of these analytical and semi-analytical models is the possibility if tailoring them for quick and easy investigations of the effects of different parameters on the performance of membrane systems. The development of a generic model with broad applicability to membrane systems requires rigorous, robust techniques.

* Corresponding author at: Laboratoire d'ingénierie des Systèmes Biologiques et des Procédés, UMR INSA CNRS 5504, UMR INSA INRA 792, 135 avenue de Rangueil, 31077 Toulouse cedex 04, France. Tel.: +33 0561559271.
E-mail address: phillipe.schmitz@insa-toulouse.fr (P. Schmitz).

Computational Fluid Dynamics (CFD) allows flow to be modeled in complex geometries. All the studies describe computational approaches to membrane filtration performance in a single fiber for one packing density. Recently, Marcos et al. [15] experimented with a transient model based on the finite element method to simulate the flow and the concentration in an ultrafiltration unit numerically. In their study, they modeled a 50-fiber cartridge by one fiber, assuming that all the fibers had the same behavior and that the flux was equal for them all. However, no specifications were given as to the spaces between two neighboring fibers or the value of the packing density.

Yoon et al. [6] described a practical method to optimize the design parameters of a vertically mounted submerged hollow fiber module. Their study dealt with the range of outer fiber diameters, the range of fiber lengths and the lumen: outer diameter ratio. A part of their study dealt with the effect of varying the outer and lumen diameters for a fixed fiber length. Assuming a regularly spaced arrangement of the fibers in the module, the authors distinguished some optimal parameters to increase filtration performance. However, reducing fiber diameter to increase packing density reduced the permeate flow rate per unit surface area. Furthermore, the membrane surface area was used less effectively at lower fiber diameters because the change in flux along the fiber length was then higher.

Chang and Fane [7] studied the effect of fiber diameter on filtration and flux distribution experimentally for hollow fiber modules under air flow bubbling. A minor part of their investigation referred to fiber arrangement. Two kinds of arrangement were proposed: the fibers were fixed in a channel with controlled spacing, or were concentrated in the centre of the channel. These two arrangements were studied with four and eight fibers and for two channel widths (24 and 8 mm). They showed an effect of increased fiber density on the decrease rate of flux decline. They linked this phenomenon with a decrease in bubble size and an unfavorable inter-fiber hydrodynamic environment.

The purpose of another study by the same authors [16] was to assess the effect of fiber orientation on the performance in the case of biomass filtration. The effect of fiber spacing on flux decline in the filtration of yeast suspension using 0.65 and 2.7 mm outer diameter fibers without bubbling was investigated. However, the smallest distance between fibers was 3 mm and did not represent the inter-fiber distances typically found in high packing density and in hollow fiber modules.

The originality of the present study is to focus on the impact of a large range of packing density on filtration performance in the case of a single-phase fluid without particles. The Navier Stokes and Darcy Brinkman equations are coupled and solved in a two-dimensional axisymmetric model to simulate fluid flow and the filtration velocity variations along a single fiber of the microfiltration module for different packing densities. For this large range of packing density, the numerical approach is studied for two modes of filtration: inside/out and outside/in. The model allows to simulate the flow in the case of an experimental device previously described [17]. The simulation results are then compared to two experimental cases corresponding to two packing densities.

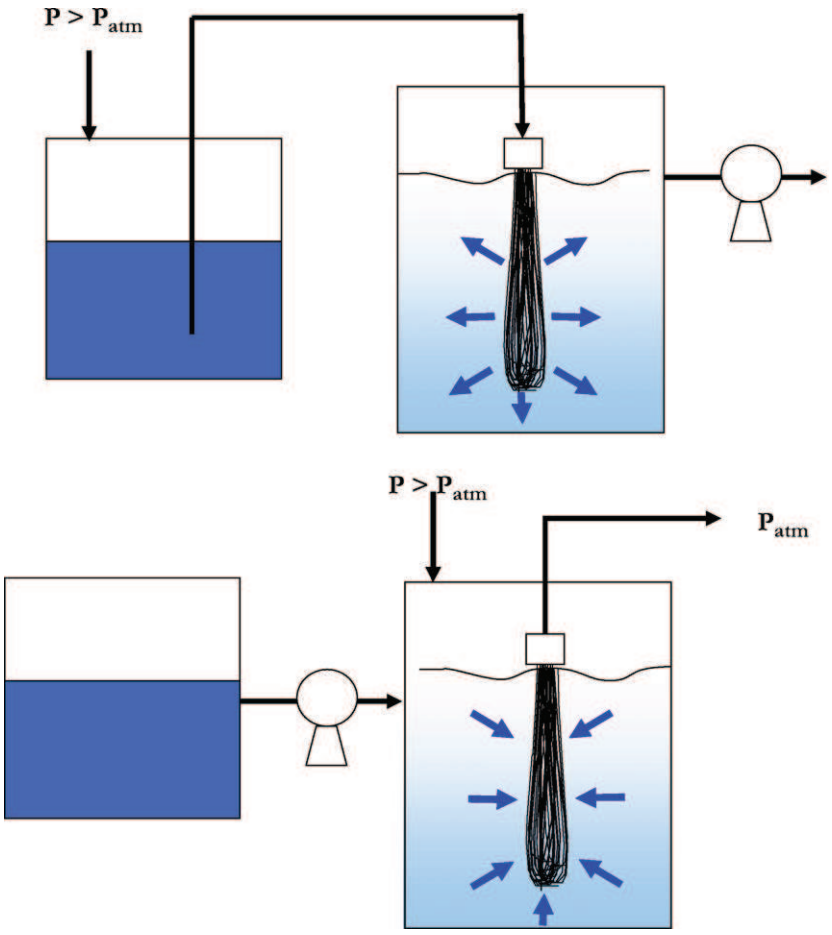

Fig. 1. Schematic design of the hollow fiber microfiltration module. (top) Inside/out filtration mode IO; (bottom) outside/in filtration mode OI.

2. Materials and methods

2.1. Experimental device

The numerical simulations were compared to some experimental results obtained with a device corresponding to a hollow fiber module immersed in a reactor filled with water. The transmembrane pressure was maintained with compressed air (Fig. 1). This system could be used both in inside/out (IO) or outside/in (OI) filtration mode, depending on the compression sense (Fig. 1). Water level in the reactor was maintained through a level regulation system that drove a feeding or draining pump. All experiments were performed at $T = 25\,^{\circ}C$.

Two bundles with different packing densities were specifically designed for this study (Polymem Toulouse, France). Their mean packing densities were $33 \pm 5\%$ and $66 \pm 5\%$. Fibers were U-shaped and were held together with epoxy-resin at their upper part. The upper part of the bundle was contained in a stainless steel punched receptacle and the filtering part immersed freely in the liquid. Fibers were made of polysulfone and had a nominal pore diameter of 0.1 μm, while the internal and external diameters were 0.25 mm and 0.43 mm respectively.

2.2. Definition of the model used for numerical simulations

Studying a system composed of a large number of single elements, such as fibers in a filtration module, is quite difficult and remains a classic problem in chemical engineering. The determination of the properties of concentrated dispersions [18] or the computation of effective properties of a porous medium [19] are typical examples and a simplification of the geometry that has been the path followed by many researchers. To estimate the different microscopic characteristic parameters in a filtration module for different packing densities, the module first has to be divided into sub-cells. A few studies report shell side mass transfer performance of random arrangements of hollow fiber membranes [20,21] and use Voronoi tessellation, which is a mathematical method to describe the subdivision of space between randomly packed objects by drawing straight boundaries equidistant between neighboring objects to form polygonal cells. However, when the Voronoi cells or the polygons are irregular, it is difficult to give the velocity profiles in the cell. In this paper, the hollow fiber bundle is modeled as an arrangement of perfectly regular cylinders and the fluid flow is calculated on the basis of a unit cell of this arrangement.

This principle comes from Happel's free surface model [22,23], initially developed to calculate the permeability of a regular stacking of fibers or derived models. This model is based on the idea that two concentric cylinders can serve as the model for fluid flowing through an assemblage of cylinders. The inner cylinder consists of one of the fibers in the assemblage of radius, R_{ext}, and the outer cylinder is a fluid envelope with a free surface of radius ($R_{ext} + D$) (Fig. 2). The relative volumes of fluid and solid in the cell model are taken to be the same as the relative volumes of fluid and solid in the assemblage of cylinders. More precisely, it is assumed that, at a distance from the disturbance to fluid motion caused by a cylinder, i.e. a fiber, the velocity of flow will not be greatly affected by the exact shape of the outside boundary. Using Happel's free surface model means that it's assumed that each hollow fiber of the module has the same average contribution to filtration performance. Thus this strong assumption is naturally associated with (i) a regular packing and (ii) a uniform distribution of flow conditions in radial cross-sections. The important consideration of this simplified approach is that the appropriate boundary condition of no slip along walls of the fluid envelope is maintained [22]. The situation is easily visualized in Fig. 2 (right), which shows the unit cell model assumed for axial flow. The fluid flows in the annular space between the cylinder of radius R_{ext} and the fluid envelope of thickness D. These boundary conditions give:

$$Vz = 0 \quad \text{at } r = R_{ext} \tag{1}$$

$$\frac{dVz}{dr} = 0 \quad \text{at } r = R_{ext} + D \tag{2}$$

2.2.1. Geometry of the system and computational mesh used

The work presented here uses the commercially-available finite element code COMSOL multiphysics™ in order to solve the coupled physical problem of flow in channels and in a porous wall. The fluid is Newtonian. We consider a stationary, laminar and incompressible flow in the fluid channels (Fig. 3, sub-domains I and E) where the Navier Stokes equations reflecting the mass and momentum balances can be solved:

$$\nabla \cdot \vec{v} = 0 \tag{3}$$

$$\rho(\vec{v} \cdot \nabla)\vec{v} = -\nabla P + \mu \nabla^2 \vec{v} \tag{4}$$

where $\vec{v}$ is the fluid velocity, P the pressure, and μ is the dynamic viscosity. The Darcy Brinkman model, an extended Darcy model reflecting the ability of flow to transmit a force through the viscous constraint in the case of high permeability, is used and the equations are solved for the numerical computation in the porous medium:

$$\mu_{eff} \Delta \vec{v} - \vec{\nabla} P - \frac{\mu}{K} \vec{v} = 0 \tag{5}$$

$$\vec{\nabla} \cdot \vec{v} = 0 \tag{6}$$

where μ_{eff} is the effective dynamic viscosity, classically considered as μ/ε, ε representing the porosity of the porous sub-domain, and K is the intrinsic permeability of the porous sub-domain (Fig. 3, sub-domain M).

In order to formulate the model, the flow is considered as a single-phase and the fibers are immobile. A typical geometry of the hollow fiber module is shown in Fig. 4: the module is assumed to be cylindrical; the cross-section is normal to the main flow in inner to outer filtration mode and is parallel in outside/in mode. A geometric domain is considered which consists of a single fiber surrounded by a fluid layer.

2.2.2. Evaluation of packing density

Packing density can be defined as the ratio of total surface area of membrane to the cross-sectional area of the module [24]. According to this definition, for a fixed fiber length and lumen, packing

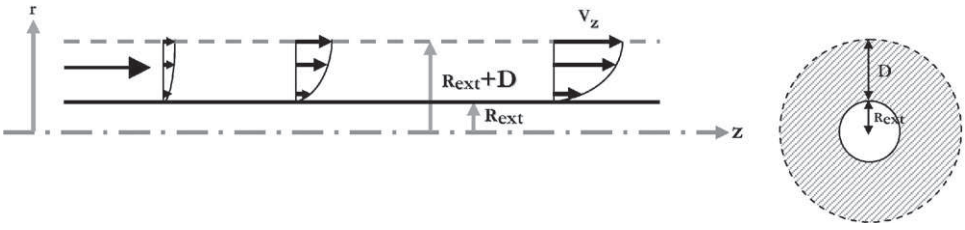

Fig. 2. Illustration of (left) fluid flow through the annular space (flow is axisymmetric so only half of the tube is represented) and (right) free surface model for axial flow.

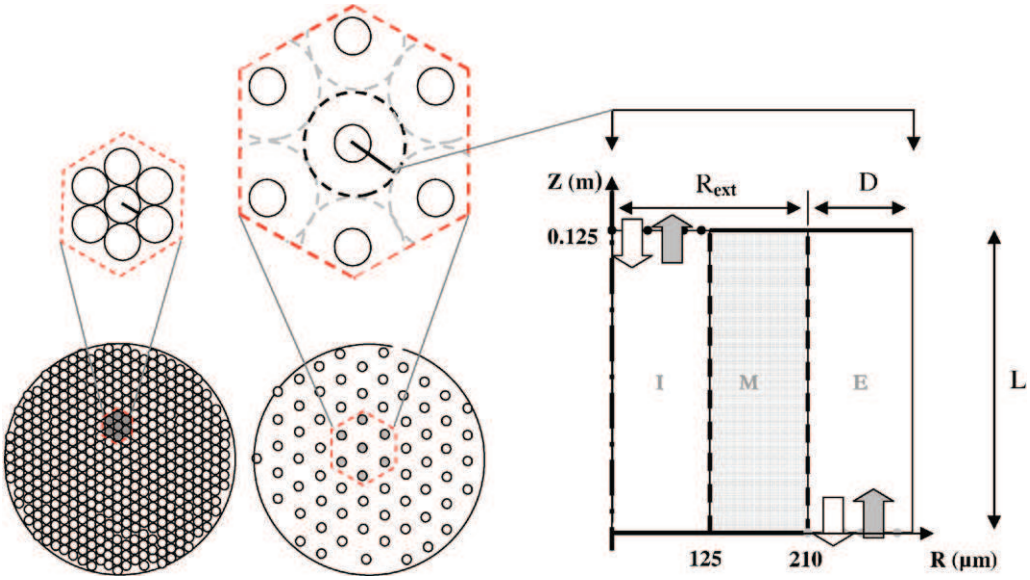

Fig. 3. Geometrical simplification of the hollow fiber bundle and scheme of the model with I: internal channel, M: membrane, E: external channel, R_{ext}: outer radius, D: distance between two fibers, and L: length of the fiber.

density increases proportionally with fiber number. However, if more fibers are used in order to increase permeate productivity, the distance between two neighboring fibers should also be kept sufficient to minimize the confinement effect and to maintain the hydrodynamic conditions within the fiber bundles.

The fiber density is determined by considering the module as a regular arrangement of discs in a plane. Thus, by taking a hexagonal optimal stacking arrangement (Fig. 4), the basic mesh is a rhombus having the four neighboring discs as vertices. Its surface area is then:

$$S_l = 2R_{ext}\left(2R_{ext}\frac{\sqrt{3}}{2}\right) = 2\sqrt{3}R_{ext}^2 \tag{7}$$

and contains the equivalent of a disc (R_{ext} is the outer radius of a fiber). The proportion of area covered, i.e. the fiber density can be written:

$$\Phi = \frac{\pi R_{ext}^2}{2\sqrt{3}(R_{ext}+D)^2} \tag{8}$$

2.2.3. Parameters for numerical application and selection of boundary conditions

2.2.3.1. Parameters. For the numerical application, the parameter values corresponded to those of the experimental device and different external channel width values were considered in order to represent the variable packing density (Table 1).

Typically, meshes with 100 cells along the fiber, 20 cells across the inner channel, and 10 cells across the porous medium were used. For the external annular channel, 5 cells, 10 cells and 20 cells were used for $D = 25\,\mu m$, $D = 50\,\mu m$ and $D = 100\,\mu m$ respectively. Moreover, a non-uniform mesh distribution was used for

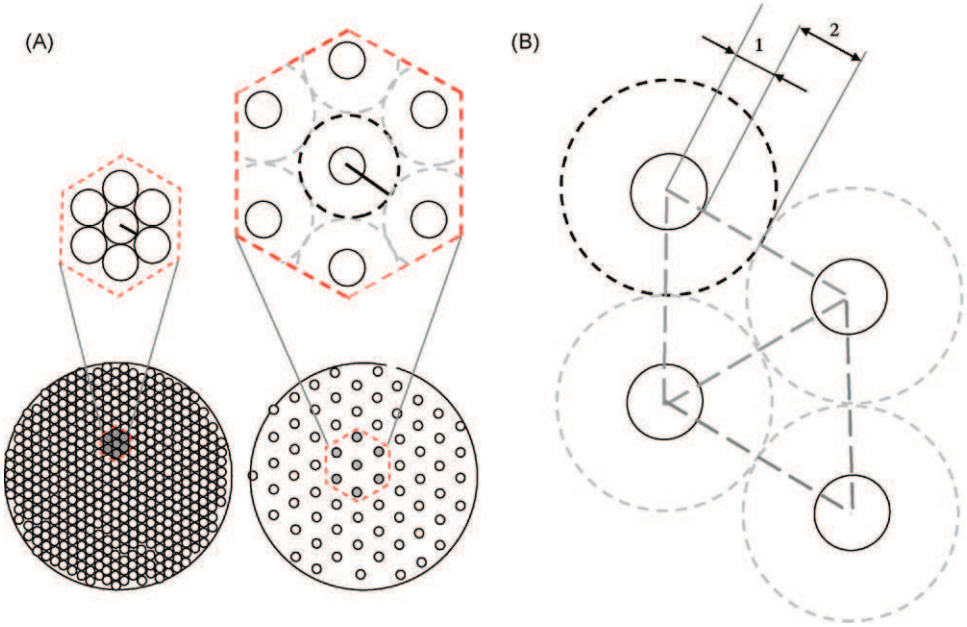

Fig. 4. (A) Schematic representation of high and low packing density in hexagonal stacking and (B) basic mesh used in the study (Rhombus) with $R_{ext} \geq 1$ and $D \geq 2$, vertices are the four neighboring discs.

Table 1
Summary of parameters values used for numerical model.

Hollow fiber
Internal radius, $R_{int} = 125e^{-6}$ m
External radius, $R_{ext} = 210e^{-6}$ m
Length, $L = 0.125$ m
Porous wall
Permeability, $K_m = 1.7e^{-16}$ m^2 (value of permeability in the experimental device)
Thickness, $e_m = 85$ μm
External channel thickness
$D = 25e^{-6}$ m for $\Phi = 0.8$
$D = 50e^{-6}$ m for $\Phi = 0.6$
$D = 100e^{-6}$ m for $\Phi = 0.4$
Transmembrane pressure $\Delta P = 0.8$ bar (value of transmembrane pressure applied in the experimental device)

the internal and external channel, with the cell density being higher at the membrane interface. Special care was taken to avoid excessively high cell stretch rates. In all three cases, we checked that the filtration velocity profile along the fiber and flow rate for the external channel was independent of the mesh used. When a mesh one fifth of the original size was used, the difference was less than 0.2% for the filtration velocity and 0.04% for the flow rate.

2.2.3.2. Boundary conditions. At the inlet, a uniform pressure condition of 0.8 bar with perpendicular flow was set.

- Inside/out filtration mode (IO): for $z = 0.125$ m, $P = 0.8$ bar.
- Outside/in filtration mode (OI): for $z = 0$ m, $P = 0.8$ bar.

Other inlet pressure or flow conditions could be specified for different applications with appropriate modification of the inlet channel width if required. At the outlet (gray small dotted line for inside/out filtration mode and black small dotted line for outside/in filtration mode in Fig. 3), the pressure was set to zero.

- IO: for $z = 0$ m, $P = 0$.
- OI: for $z = 0.125$ m, $P = 0$.

Axisymmetric, for $r = 0$, $V_r = 0$ (and vanishing stresses in z direction) and symmetric boundaries are set in dotted and thin solid black lines respectively (Fig. 3).

At both the non-porous and porous walls (solid black), the no slip condition was imposed. It is true that the boundary condition at the fluid/porous medium interface is still an open question for specialists. Beavers and Joseph [25] proposed a slip condition at the interface for the coupling between a Navier Stokes model for fluid flow in the channels and a Darcy Brinkman model in the porous medium (porous wall). On the microscopic scale, the surface of the porous medium consists of solid wall, on which fluid sticks and pores, on which fluid slips. Therefore, even though the Darcy Brinkman model considers a homogeneous surface, the physical behavior of the fluid has to be taken into account using a slip condition. However, it has been found in a previous paper [26] that the slip velocity at the interface can be neglected as long as the permeability of the porous medium is low, i.e. the aspect ratio between the pore diameter and the height of the channel is small. As this is the case for a hollow fiber, it can be assumed that there is no slip velocity at the fluid/porous medium interface. Thus, it remains the continuity of the normal velocity and the pressure at the interface. They are represented in large black dotted line (Fig. 3).

3. Results and discussion

With the geometrical model presented previously, numerical results were obtained for different module configurations corresponding to three values of the packing density.

For inside/out filtration mode, the profile of the axial velocity in the unit cell for three sections ($z = 6.4e^{-3}$, 0.056 and 0.12 m) are given in Fig. 5 for the lumen and in Fig. 6 for the external channel. For outside/in filtration mode, Figs. 7 and 8 show the axial velocity profile of the external channel and the lumen, respectively, for the three sections described above. As can be seen, all the velocity profiles are parabolic. This is similar to the classical velocity profile obtained for a fully developed laminar flow in a channel without wall suction or injection. A number of authors have already studied fluid flow in various channels with wall suction or injection [27,28].

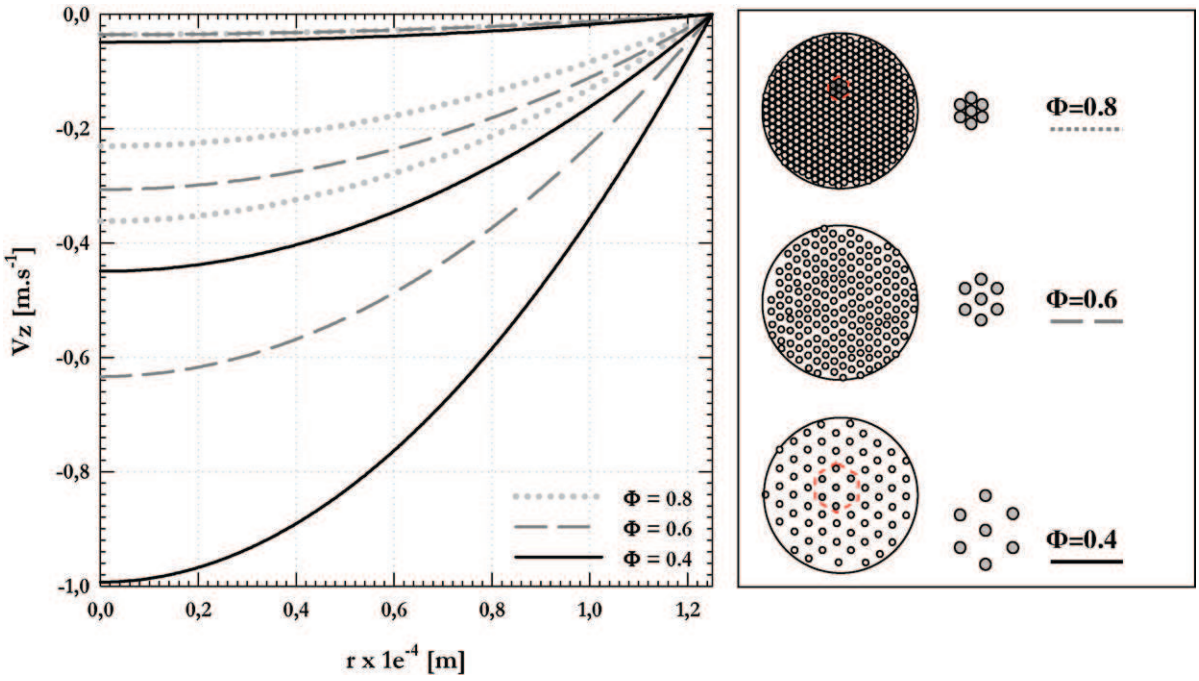

Fig. 5. Velocity profiles in the lumen versus width at $z = 6.4e^{-3}$, 0.056 and 0.12 m, in the inner to outer filtration mode.

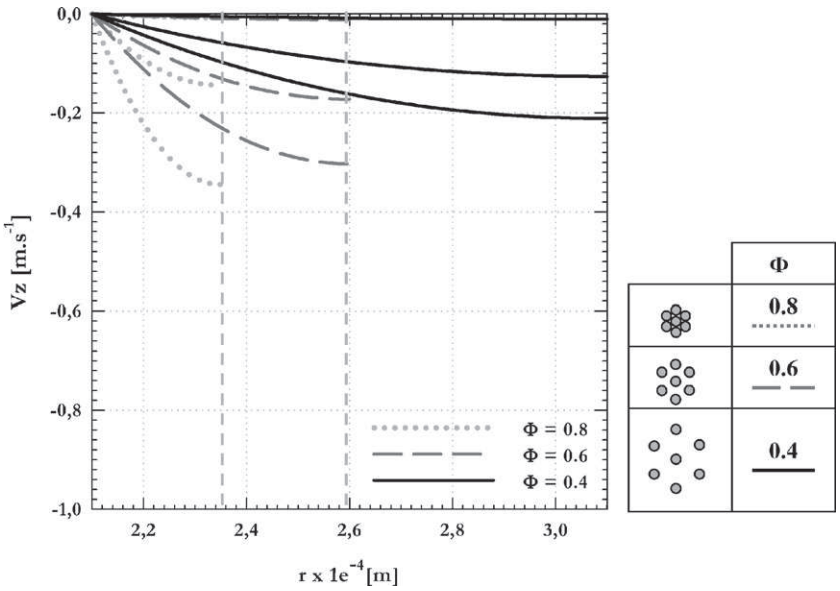

Fig. 6. Velocity profiles in the external channel versus width at $z = 6.4e^{-3}$, 0.056 and 0.12 m, in the inner to outer filtration mode (dotted lines are the geometrical axis of symmetry of each model).

Similar solutions of fully developed laminar flows have been developed for low [29,30] and high [31,32] wall suction and injection. The critical parameter is Re_w, the wall Reynolds number based on filtration velocity and channel half height. It should be noted that in the present study the velocity profile obtained is found to be approximated fitted by a parabolic profile as could be expected since Re_w is always lower about 0.01. Thus the numerical results obtained confirm the previous theoretical investigations.

Several observations can also be made. Considering IO mode and a fixed packing density, as can be expected, while retentate flows from the inlet to the bottom of the fiber, the flow velocity increases in the inner channel and in the external channel (permeate side). While permeate flows towards the exit, additional permeate is added to the flow and the flow velocity increases in the external channel. Consequently, the rate of pressure drop should increases along the fiber. Regarding increasing packing density, with space restriction in the external channel, the flow velocity decreases in the internal channel and increases on the permeate side. For OI filtration mode, the space restriction acts in the opposite way in the external channel; i.e. it enhances the increase of flow velocity with the packing density. Consequently the rate of decrease in pressure drop should be greater for a high packing density than for a weak packing density.

In order to assess the significance of the pressure variation along the fiber in both the internal and the external channel, the pressure P is shown in Figs. 9 and 10 for three values of the packing density. For IO filtration mode, considering packing densities of $\Phi = 0.8$ (high), $\Phi = 0.6$ and $\Phi = 0.4$ (low), the pressure drops in the retentate side (Ret.) reach 0.04 bar, 0.09 bar and 1.5 bar respectively. Regarding the permeate side, for $\Phi = 0.8$, 0.6 and 0.4, the pressure drops reach 0.56 bar, 0.13 bar and 0.01 bar respectively. Introducing the local transmembrane pressure ΔP_l, which is the difference

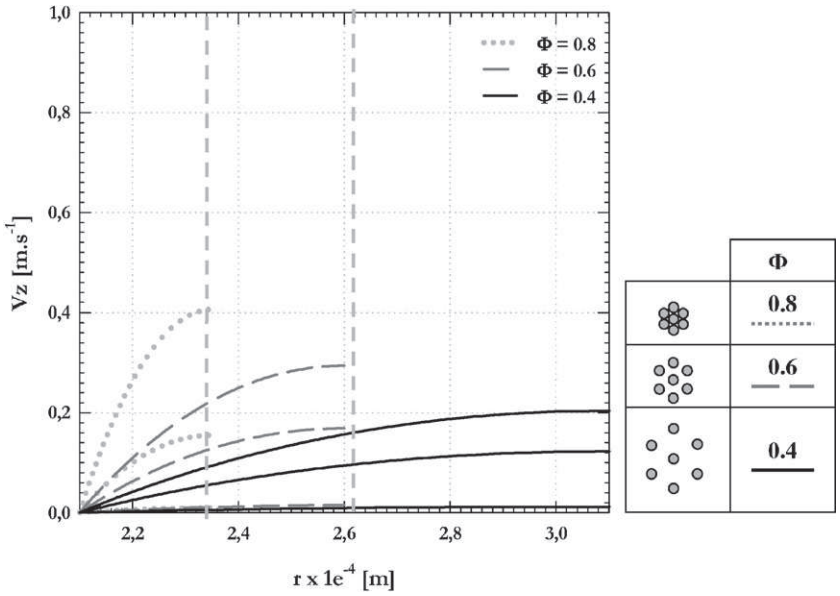

Fig. 7. Velocity profiles in the annulus versus width at $z = 6.4e^{-3}$, 0.056 and 0.12 m, in the outside/in filtration mode (dotted lines are the geometrical axis of symmetry of each model).

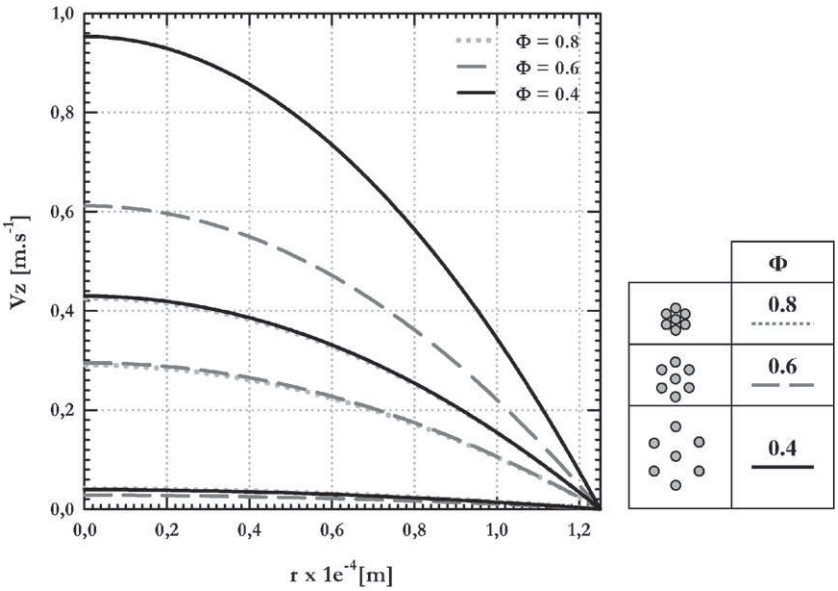

Fig. 8. Velocity profiles in the internal channel versus width at $z = 6.4e^{-3}$, 0.056 and 0.12 m, in the outer to inner filtration mode (dotted lines are the geometrical axis of symmetry of each model).

between the pressures at the retentate and permeate sides for a fixed z coordinate ($\Delta P_l = P_R - P_P$) (taking into account manometric pressure variation), this term is 70% lower at the top than at the bottom of the fiber for $\Phi = 0.8$. Lower values of Φ lead to a decrease in this difference between the top and bottom of the fiber.

Regarding OI filtration mode, for $\Phi = 0.8$, 0.6 and 0.4, the pressure drops in the retentate side at the top of the fiber are 0.04 bar, 1.5 bar and 0.63 bar respectively. Values for the permeate side reach 0.1 bar, 0.12 bar and 0.17 bar at the bottom of the fiber for packing densities of 0.8, 0.6 and 0.4 respectively. The local transmembrane pressure difference between the top and the bottom of the fiber reaches 80% for high packing density. The variation of pressure along the fiber is dictated by the confinement of the system. As the diameter decreases with increasing packing densities, the variation of local transmembrane pressure drop becomes greater.

At the membrane surface, the filtration velocities along the fiber length for the different packing densities are shown in Figs. 11 and 12 for inside/out and outside/in filtration mode respectively. These variations are the direct consequence of variations of pressure along the fiber at both the retentate and permeate sides, which are proportional to the local transmembrane pressure. Regarding inner to outer filtration mode and $\Phi = 0.8$, filtration velocity at the entrance of the fiber is 72% lower than at the outlet. Filtration velocity is almost uniform along the fiber length for $\Phi = 0.6$. For a weak packing density $\Phi = 0.4$, the inside/out filtration mode leads to a higher filtration velocity at the top (entrance) of the fiber. The outside/in filtration mode shows the opposite filtration velocity profile, i.e. a higher filtration velocity at the bottom (entrance) than at the top of the fiber, and presents higher filtration velocity. For $\Phi = 0.8$, 0.6, and 0.4, the differences between filtration velocity values found at the entrance and at the bottom of the fiber reach values of 28%, 12.5% and 18% respectively. Thus, an increase of the filtration velocity is mainly due to an increase in local transmembrane pressure from the entrance to exit. This

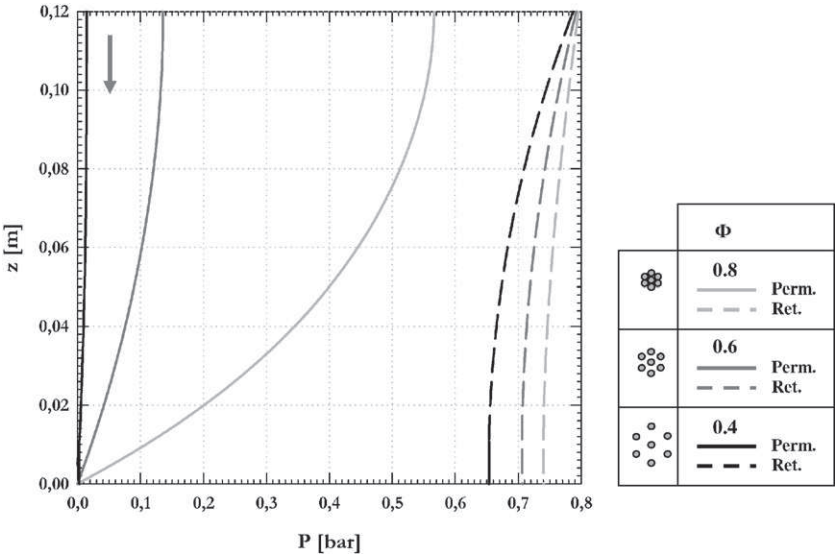

Fig. 9. Variation of pressure along the fiber at the permeate side (permeate side, solid line) and at the retentate side (retentate side, dashed line) for inner to outer filtration mode.

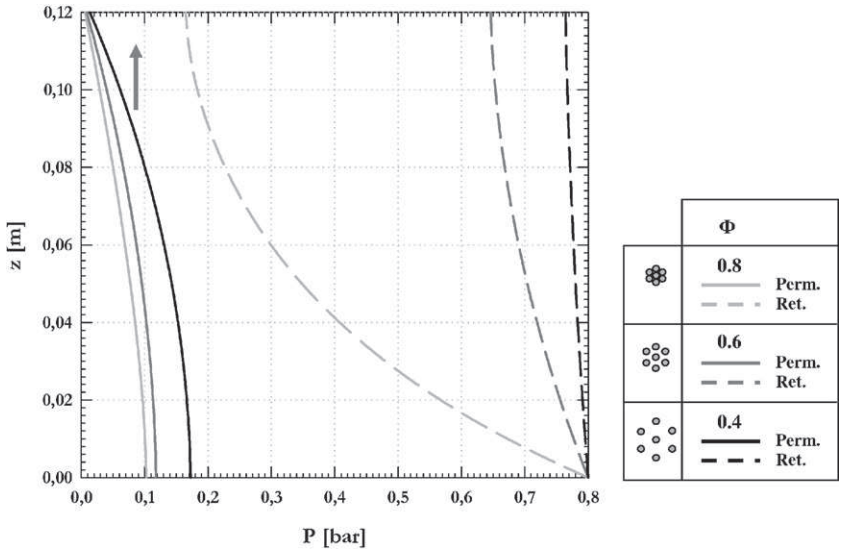

Fig. 10. Variation of pressure along the fiber at the permeate side (permeate side, solid line) and at the retentate side (retentate, dashed line) for outer to inner filtration mode.

phenomenon could significantly reduce membrane performance, i.e. performance levels predicted using models assuming uniform filtration velocity.

To sum up, in inner to outer filtration mode, the space restriction in the annulus due to the increase in packing density leads to a higher pressure at the top of the external channel than at the bottom, generating a high gradient of local transmembrane pressure along the fiber. Filtration takes place preferentially in the region where the transmembrane pressure is highest, i.e. at the bottom of the fiber. As the distance between two neighboring fibers grows, the profile of local transmembrane pressure drop reverses more and filtration occurs at the top of the fiber. Exactly the same phenomenon occurs in the outside/in filtration mode. A higher transmembrane pressure at the bottom of the fiber will lead to a higher filtration flux, generating a non-uniform filtration flux profile.

Fig. 13 shows the evolution of filtration flux with packing density and compares numerical and experimental data in outside/in filtration mode. Firstly, this representation clearly illustrates the dramatic effect on filtration performance of increasing the packing density. Secondly, Fig. 13 shows a very good agreement between numerical and experimental results in terms of net filtration flow rate validating the 2D dimensional simplification with Happel's free surface model. The packing density induces longitudinal variation of filtration velocity along the fiber length. For high density of fiber, preferential filtration velocity is found on the bottom of the fiber in inside/out and in outside/in filtration mode.

This last point provides a very interesting way of investigating the polarization layer or fouling in the case of filtration of a particle suspension [33]. With the assumption that particles follow the streamlines, spatial variation of thickness could be observed all along the fiber length and this last point will be presented in our forthcoming studies. Moreover, there are a few prospects for studying the impact of packing density on growth and longitudinal distribution of the fouling cake.

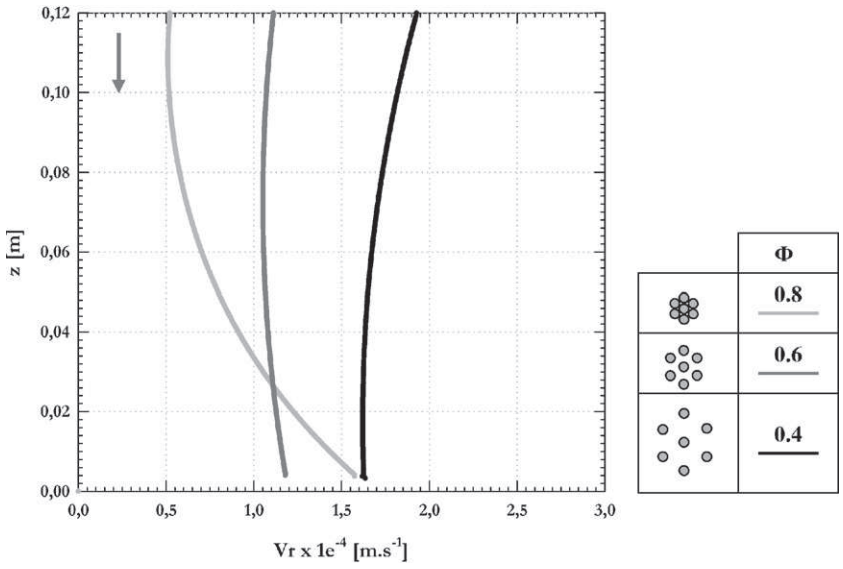

Fig. 11. Filtration velocity along the fiber in inner to outer filtration mode.

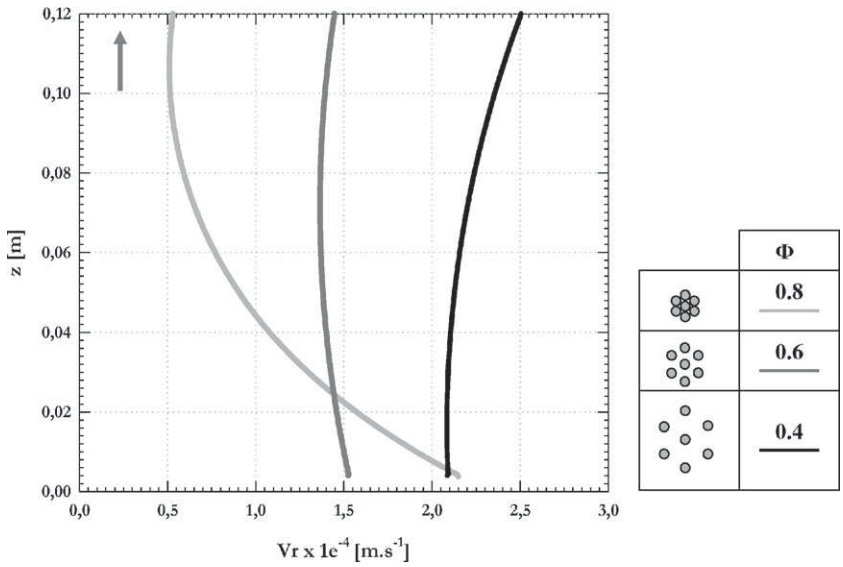

Fig. 12. Filtration velocity along the fiber in outer to inner filtration mode.

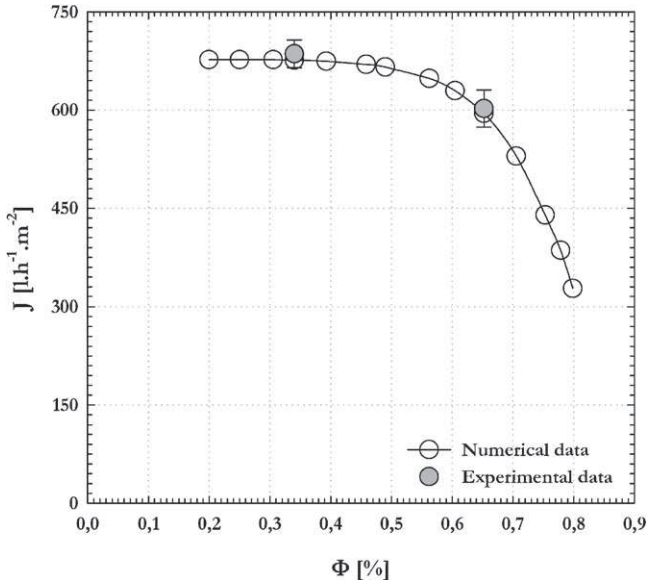

Fig. 13. Evolution of filtration flux with packing density.

4. Conclusion

The CFD based model developed in this study demonstrates its entire handling to study the impact of geometrical parameters of a hollow fiber module on filtration performance levels. The results underline the major effect of packing densities on filtration velocity and, particularly, on the spatial distribution of permeate velocity along the whole fiber length. Although the effect of particle capture and eventual movement of the fiber bundle in the module are neglected in this work, the model was able to predict that: (i) increasing packing density would lead to a non-uniform permeate profile along the fiber length, (ii) at very high packing density, filtration flux would decrease dramatically and (iii) filtration would occur preferentially at the bottom of the fiber. While the CFD model developed contains a fixed lumen radius, the geometry can be easily modified to encompass any fiber lumen and fiber external radii found in the literature. Some investigations of the spatial deposition of deposit cake have been undertaken, and will be presented in a forthcoming study.

Nomenclature

E	external channel sub-domain
I	internal channel sub-domain
Perm.	permeate side
Ret.	retentate side
IO	inside/out filtration mode
OI	outside/in filtration mode
D	thickness of the fluid envelope (m)
K	intrinsic permeability (m^2)
L	length of the fiber (m)
M	membrane or porous sub-domain
P	pressure (bar)
P_p	pressure of permeate side (bar)
P_r	pressure of retentate side (bar)
R_{ext}	fiber radius (m)
Re_w	wall Reynolds number

Greek symbols

ΔP_l	local transmembrane pressure (bar)
ε	porosity
μ	dynamic fluid viscosity (Pa s)
μ_{eff}	effective dynamic fluid viscosity (Pa s)
Φ	packing density (%)

References

[1] A.P.S. Yeo, A.W.K. Law, A.G. Fane, Factors affecting the performance of a submerged hollow fiber bundle, J. Membr. Sci. 280 (2006) 969–982.
[2] C. Albasi, Y. Bessiere, S. Desclaux, J.C. Remigy, Filtration of biological sludge by immersed hollow-fiber membranes: influence of initial permeability choice of operating conditions, Desalination 146 (2002) 427–431.
[3] J. Busch, A. Cruse, W. Marquardt, Modeling submerged hollow-fiber membrane filtration for wastewater treatment, J. Membr. Sci. 288 (2007) 94–111.
[4] L. De Bartolo, S. Salerno, E. Curcio, A. Piscioneri, M. Rende, S. Morelli, F. Tasselli, A. Bader, E. Drioli, Human hepatocyte functions in a crossed hollow fiber membrane bioreactor, Biomaterials 30 (2009) 2531–2543.
[5] B. Girard, L.R. Fukumoto, Membrane processing of fruit juices and beverages: a review, Crit. Rev. Food Sci. Nutr. 40 (2000) 91–157.
[6] S.-H. Yoon, H.-S. Kim, I.-T. Yeom, Optimization model of submerged hollow fiber membrane modules, J. Membr. Sci. 234 (2004) 147–156.
[7] S. Chang, A.G. Fane, The effect of fibre diameter on filtration and flux distribution—relevance to submerged hollow fibre modules, J. Membr. Sci. 184 (2001) 221–231.

[8] J. Zheng, Y. Xu, Z. Xu, Flow distribution in a randomly packed hollow fiber membrane module, J. Membr. Sci. 211 (2003) 263–269.
[9] S. Chang, A.G. Fane, T.D. Waite, A. Yeo, Unstable filtration behavior with submerged hollow fiber membranes, J. Membr. Sci. 308 (2008) 107–114.
[10] A. Yeo, A.G. Fane, Performance of individual fibers in a submerged hollow fiber bundle, Water Sci. Technol. 51 (2005) 165–172.
[11] S.K. Karode, Laminar flow in channels with porous walls, revisited, J. Membr. Sci. 191 (2001) 237–241.
[12] W.N. Gill, D.E. Wiley, C.J.D. Fell, A.G. Fane, Effect of viscosity on concentration polarization in ultrafiltration, AIChE J. 34 (1988) 1563–1567.
[13] S.-H. Yoon, S. Lee, I.-T. Yeom, Experimental verification of pressure drop models in hollow fiber membrane, J. Membr. Sci. 310 (2008) 7–12.
[14] V. Nassehi, Modelling of combined Navier–Stokes and Darcy flows in crossflow membrane filtration, Chem. Eng. Sci. 53 (1998) 1253–1265.
[15] B. Marcos, C. Moresoli, J. Skorepova, B. Vaughan, CFD modeling of a transient hollow fiber ultrafiltration system for protein concentration, J. Membr. Sci. in press.
[16] S. Chang, A.G. Fane, S. Vigneswaran, Experimental assessment of filtration of biomass with transverse and axial fibres, Chem. Eng. J. 87 (2002) 121–127.
[17] J. Günther, C. Albasi, C. Lafforgue, Filtration characteristics of hollow fiber microfiltration membranes used in a specific double membrane bioreactor, Chem. Eng. Process: Process Int. in press.
[18] T.F. Tadros, Use of viscoelastic measurements in studying interactions in concentrated dispersions, Langmuir 6 (1990) 28–35.
[19] B. Nétinger, The effective permeability of a heterogeneous porous medium, Trans. Porous Media 15 (1994) 99–127.
[20] Y. Wang, F. Chen, Y. Wang, G. Luo, Y. Dai, Effect of random packing on shell-side flow and mass transfer in hollow fiber module described by normal distribution function, J. Membr. Sci. 216 (2003) 81–93.
[21] J.D. Rogers, R.L. Long, Modeling hollow fiber membrane contactors using film theory, Voronoi tessellations, and facilitation factors for systems with interface reactions, J. Membr. Sci. 134 (1997) 1–17.
[22] J. Happel, Viscous flow relative to arrays of cylinders, AIChE J. 5 (1959) 174–177.
[23] J. Happel, H. Brenner, Low Reynolds Number Hydrodynamics, Noordhoof, Leyden, The Netherands, 1983.
[24] S. Chang, A.G. Fane, S. Vigneswaran, Modeling and optimizing submerged hollow fiber membrane modules, AIChE J. 48 (2002) 2203–2212.
[25] G.S. Beavers, D.D. Joseph, Boundary conditions at a naturally permeable wall, J. Fluid Mech. Dig. Arch. 30 (1967) 197–207.
[26] M. Prat, P. Schmitz, 3-D laminar stationary flow over a porous surface with suction: description at pore level, AIChE J. 41 (1995) 2212–2226.
[27] S.G. Chatterjee, G. Belfort, Fluid flow in an idealized spiral wound membrane module, J. Membr. Sci. 28 (1986) 191–208.
[28] L. Oxarango, P. Schmitz, M. Quintard, Laminar flow in channels with wall suction or injection: a new model to study multi-channel filtration systems, Chem. Eng. Sci. 59 (2004) 1039–1051.
[29] A.S. Berman, Laminar flow in channels with porous walls, J. Appl. Phys. 24 (1953) 1232–1235.
[30] S.W. Yuan, A.B. Finkelstein, Laminar pipe flow with injection and suction through a porous wall, Trans. ASME 78 (1955) 719–724.
[31] R.M. Terril, Laminar flow in a uniformly porous channel, Aeronautical (1964) 297.
[32] R.M. Terril, Laminar flow in a porous tube, J. Fluids Eng. 105 (1983) 303–307.
[33] K. Damak, A. Ayadi, B. Zeghmati, P. Schmitz, Concentration polarisation in tubular membranes—a numerical approach, Desalination 171 (2005) 139–153.